NANOSYSTEMS:
PHYSICS, CHEMISTRY, MATHEMATICS

Ayesh A.I. *Nanosystems: Phys. Chem. Math.*, 2025, **16** (4), 450–459.
http://nanojournal.ifmo.ru
DOI 10.17586/2220-8054-2025-16-4-450-459

Original article

Half-metallic dichalcogenide doped with a transition metal for selective gas adsorption

Ahmad I. Ayesh[1,a]

[1]Department of Physics and Materials Sciences, College of Arts and Sciences, Qatar University, P.O. Box 2713, Doha, Qatar

[a]ayesh@qu.edu.qa

Corresponding author: A. I. Ayesh, ayesh@qu.edu.qa

ABSTRACT The half metallic transformation of MoSeS dichalcogenide structure upon doping with a transition metal is explored in this work. Additionally, the effect of doping on its adsorption capacity for CO, CO_2, NO, and NO_2, H_2, H_2O, H_2S, and NH_3 gases is investigated. Those gases are considered due to their impact on the greenhouse effect as well as climate change. Density functional theory (DFT) and first principles computation are utilized to evaluate the effect of Fe doping of MoSeS structure on the adsorption energy (E_a) and length (d), charge relocated between gas molecules and the structure (Δq), along with the density of states (DOS). The results reveal that Fe doping of MoSeS structure generates significant adjustments of the band gap so that the structure could be transformed from semiconductor into metallic or semimetallic. NO, NO_2, and O_2 gases exhibit favorable adsorption on doped structure with a maximum adsorption capacity for NO. Additionally, the doped structure exhibits selective adsorption for the gases with different adsorption energies. The doping of MoSeS dichalcogenide with Fe transition metal is a decent pathway to adjust its band gap along with its selectivity for gas adsorption.

KEYWORDS Transition metal, dichalcogenides, DFT, first-principles, MoSeS, gas adsorption.

FOR CITATION Ayesh A.I. Half-metallic dichalcogenide doped with a transition metal for selective gas adsorption. *Nanosystems: Phys. Chem. Math.*, 2025, **16** (4), 450–459.

1. Introduction

Two dimensional (2D) materials have been investigated intensively recently, thanks to the discovery of graphene in 2004 that initiated a massive research field on 2D materials due to their attractive technological applications [1]. Several 2D materials have been fabricated and examined, for various applications that require large band gaps, such as transition metal dichalcogenides, hexagonal BN, silicon, and others [2–4]. 2D transition metal dichalcogenides are semiconductors, and one of their possible compositions is MoXY (with X and Y = S and Se). They hold fascinating characteristics that include direct band gap, the thickness of atomic scale, strong coupling of spin orbit, along with favorable magnetic and electronic characteristics [5]. The synthesis of transition metal dichalcogenides has been demonstrated using many bottom-up and top-down approaches [6]. The properties of those materials (including band gap and magnetization) can be controlled to target specific applications [7]. Hence, transition metal dichalcogenides are considered a strategic category of materials due to their fascinating characteristics that are suitable for applications in multiple fields including spintronics, electronics, energy storage as well as harvesting, optoelectronics, DNA sequencing, chemical and gas sensing, etc. [8].

A conductometric gas sensor is a device that allows the adsorption of gases and indicates their concentrations as a variation in electrical conductance [9]. The sensitive materials of the sensors must exhibit enhanced adsorption capacities for the target gases, and their functionality has been developed in the last decade, thanks to the innovation in the synthesis of new low-dimensional materials [10]. Precise quantification of gas content in an environment, including greenhouse gases, is of crucial importance for making accurate decisions followed by actions to limit its emission. Herein, the electrical signal of a gas sensor is a feed into control as well as safety systems that take a series of programmed actions and/or processes [11].

Half metallicity is a characteristic of a class of materials that enables its utilization for spintronics applications due to switching between the metallic and semiconducting behavior upon changing the spin orientation [12]. Few approaches have been employed recently for achieving half metallicity in 2D transition metal dichalcogenides through functionalization [13], the introduction of point defects including interstitials and vacancies [14], along with other pathways [15]. Yet, doping of transition metal dichalcogenides remains a challenge due to strict requirements to form ferromagnetic order within the 2D systems [16].

Many research groups examined 2D materials with half-metallicity computationally [17]. The challenges facing the integration of 2D materials within spintronic devices and their upcoming perspective for devices on spin logic have been reported [18]. Spintronics devices of improved spin diffusion length and long spin relaxation time in transition metal

dichalcogenides have been reported recently [19]. The manipulation of spin that yielded great potential of improvement for device applications in spintronic using 2D graphene along with inorganic semiconductors has been reported by Ahn [20]. Ma et al. reported a density functional theory (DFT) investigation of MoS_2 doped using transition metal atoms (Rh, Pd, Co, Ni, Ir, Ru, Pt, and Au) at the S-site [21]. Doping with the mentioned atoms was found to induce magnetism into the partly occupied d-orbitals near the Fermi level and the corresponding lattice. Herein, doping played a vital role to increase magnetization and enhance oxygen molecule adsorption. Gas adsorption influenced the electronic structures of MoS_2 along with the magnetic characteristics. The effect of MoS_2 monolayer doping at the S-site (using Fe, Cu, Ag, Co, Ni, Au, Rh, Pt, Pd, and Ir) on its adsorption capacity of gas molecules (O_2, NO_2, CO, NO, and NH_3) has been investigated using DFT [22]. Fe was found to be an excellent dopant to enhance the selectivity and sensitivity of the above gases.

The focus of the current investigation is to utilize DFT computations to examine half metallicity of a transition metal dichalcogenide (MOSeS) 2D structure. The effect of Fe doping on its half metallicity is examined. Furthermore, the adsorption capacity of O_2, CO, CO_2, NO, NO_2, HN_3, H_2, H_2O, and H_2S gases on both pristine and doped structures is inspected. The results indicate that doping of MoSeS with Fe induces half metallicity. The source of half metallicity along with its relation to the gas sensing are examined. Herein, Fe doping of MoSeS transition metal dichalcogenide would eliminate dangling bonds and hence decrease or somewhat suppress the magnetization. Subsequently, the suppression generated for the local magnetic moment eliminates its half metallicity. Additionally, oxidizing molecules act to suppress the half metallicity of transition metal dichalcogenides, thus, they are ideal candidates for gas sensing applications [23]. The adsorption of CO, CO_2, NO, and NO_2, H_2, H_2O, H_2S, and NH_3 gases is explored by DFT computations through evaluation of density-of-states (DOS), adsorption length and energy, band structure modification, and charge relocated between gas molecules and the structure.

2. Computational method

Detailed DFT calculations were employed to examine the electronic characteristics of the new MoSeS structure, both pristine and Fe doped. Additionally, the capacity of both structures of gas adsorption was investigated [24]. A Synopsys produced simulation package (atomistic quantum (ATK)) was utilized to explore the band structure, and electronic properties, along with the adsorption parameters of MoSeS structure [25–28]. MoSeS supercell (5×5) was constructed, and then Fe doped by replacing a central Se atom. One should notice that adatom might be achieved by an atom replacement (doping), or the introduction of an additional central or bridge atom. Herein, doping was considered because it is anticipated to generate higher gas adsorption energy (the number of free bonds for the other options decreases, which reduces the probability of gas adsorption) [29]. The dope new structure was labeled as MoSeS-Fe. The exchange correlation among electrons was explored by employing the generalized gradient estimation accompanied with exchange correlation of Perdew B. Ernzerh (GGA-PBE) [30, 31]. The Van der Waals force influence was attuned by Grimme function type DFT-D2 [31]. The spin effect was counted during the investigation since it had a role in revealing the half-metallicity of the doped–pristine structures [13]. The pristine and doped structures were optimized at a temperature of 300 K using a cutoff energy Hartree mesh of 100. The minimum force tolerance and stress through the geometry optimization procedure were 0.01 eV/Å and 0.1 GPa, respectively. The Brillouin zone sampling of Monkhorst Pack was utilized for all optimization computations (i.e. geometry and electronic characteristics) at a grid with a k-point sampling of 2×2×1 [32].

The structure capacity of gas adsorption was examined by means of adsorption energy (E_a). Herein, each gas molecule was positioned above the center of MoSeS structure, where it was free to undergo translational and rotational motions. The adsorption energy of a gas molecule on the structure was evaluated as [33–35]:

$$E_a = E_{MoSeS+gas} - (E_{MoSeS} + E_{gas}) \tag{1}$$

Herein, $E_{MoSeS+gas}$ denotes the overall energy of a gas molecule adsorbed on a MoSeS structure, E_{MoSeS} denotes the overall energy of a MoSeS structure, and E_{gas} denotes the gas molecule overall energy The charge transferred amongst a gas molecule and MoSeS structure (Δq) after the gas adsorption was evaluated by the Mulliken population approach as [34, 36]:

$$\Delta q = q_f - q_i \tag{2}$$

where, q_i and q_f donate the overall Mulliken charge of a gas molecule before and following its adsorption, respectively. The impact of gas adsorption on the bandgap energy (E_g), DOS, and adsorption length between a MoSeS structure and gas molecule (d) was explored.

3. Results and discussion

Transition metal dichalcogenides of MoXY composition crystallize normally in a triangular-prismatic phase of reduced symmetry [37]. Bulk MoXY belongs to the D^4_{6h} space group, while a monolayer of its structure exhibits a reduced symmetry and belongs to the D^1_{3h} space group [37]. The reduced dimensionality and symmetry of MoXY structure cause its d states to split to three groups (according to the point-group theory): singlet state A_1', doublet state d_{xy} and d_{x2-y2}, and another doublet state d_{yz} and d_{zx}. This structure exhibits a direct band gap at the k-corner in the Brillouin zone, as well as both the minimum and maximum of the conduction and valance bands, respectively, are signified by the d state

of the transition metals with symmetries of E' and A1': the conduction band minimum is assigned to the d_{xy} and d_{x2-y2} orbitals, while the valence band maximum is assigned to the d_{z2} orbital.

The effect of Fe doping of MoSeS structure on its half metallic transformation alongside the adsorption of different gases is examined in this investigation. Fig. 1 presents monolayers of optimized pristine and Fe doped MoSeS structures. The Mo-S bond length is 2.43 Å while the Mo-Se bond length is 2.58 Å for the optimized MoSeS structures. Those bond lengths remain almost similar after Fe doping, where a Fe atom replaces a central Se atom. The electron difference density and electrostatic difference potential diagrams of pristine and Fe doped MoSeS structures are illustrated in Fig. 2. The figure indicates clear modifications of both electron difference density as well as electrostatic difference potential diagrams due to Fe doping.

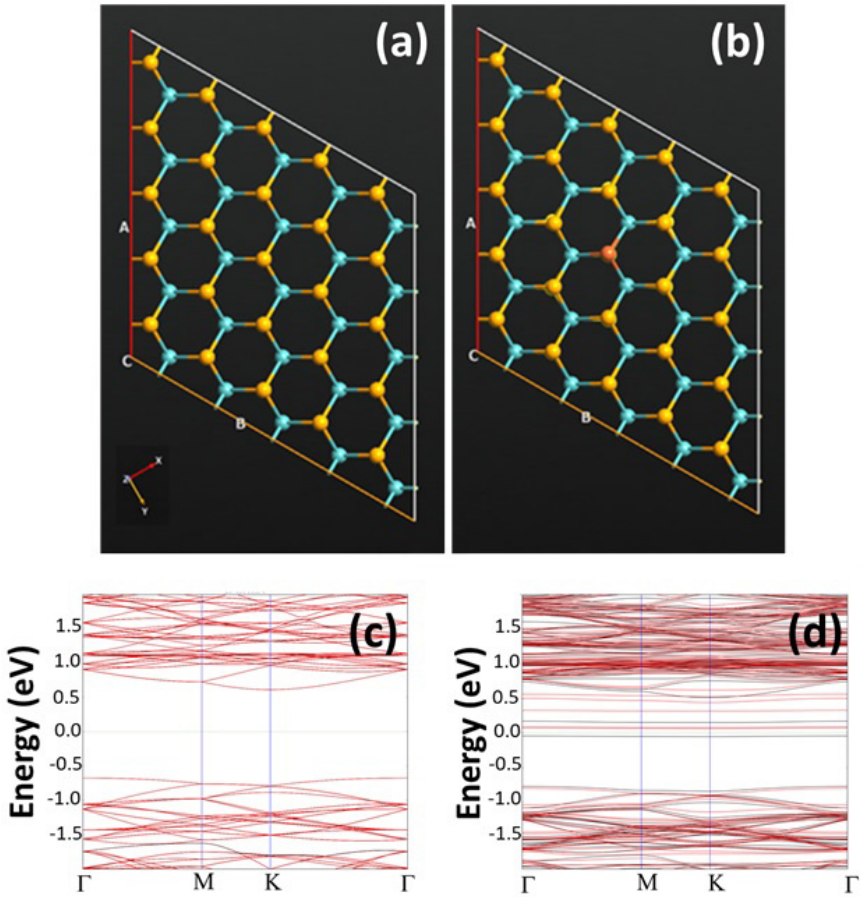

FIG. 1. Top view of MoSeS structure: a) pristine and b) Fe doped. The yellow-brown atoms are Se, yellow atoms underneath Se are S, the blue atoms are Mo, and the brown atom is Fe. The band structures for the optimized MoSeS structures: c) pristine, and d) Fe doped

Doping of an MoSeS structure with a Fe atom alters its energy levels and the subsequent band energy. Fig. 1 reveals also the band diagrams of pristine and Fe doped MoSeS. The pristine structure exhibits a semiconducting feature with a direct band gap of 1.375 eV, as presented in Table 1, that is close to the band gap energy of $MoSe_2$ of 1.42 eV [38]. Doping with Fe introduces two new main features: it decreases the band gap dramatically to the semimetallic zone with a band gap of 0.114 eV (Table 2), and more importantly, it generates configurations of exchange splitting among spin-up and spin-down states near the Fermi level indicating spin-polarized density of states.

Figure 3 presents the optimized pristine MoSeS structure upon adsorption of CO, CO_2, H_2, H_2O, H_2S, NH_3, NO, NO_2, and O_2 gases. The figure indicates that none of the gases is chemisorbed (form a chemical bond) on the structure. This is also in agreement with the large adsorption lengths ($\geq$2.67 Å) of the gases on the pristine structure as shown in Table 1. The adsorption of CO, CO_2, H_2, H_2O, H_2S, NH_3, NO, NO_2, and O_2 gases on Fe doped MoSeS structure are presented in Fig. 5. The figure demonstrates that CO, CO_2, H_2O, NH_3, NO, NO_2, and O_2 gases are chemisorbed on the structures. Table 2 indicates that the adsorption lengths of the gases on the Fe doped structures ($\leq$2.44 Å) are lower than those of the pristine structure indicating their favorable adsorption. This illustrates that the Fe doped MoSeS structure exhibits greater capacity for gas adsorption. The minimum value of adsorption length is for NO gas, while H_2S exhibits the maximum adsorption length in qualitative support of the chemisorption observations in Fig. 4.

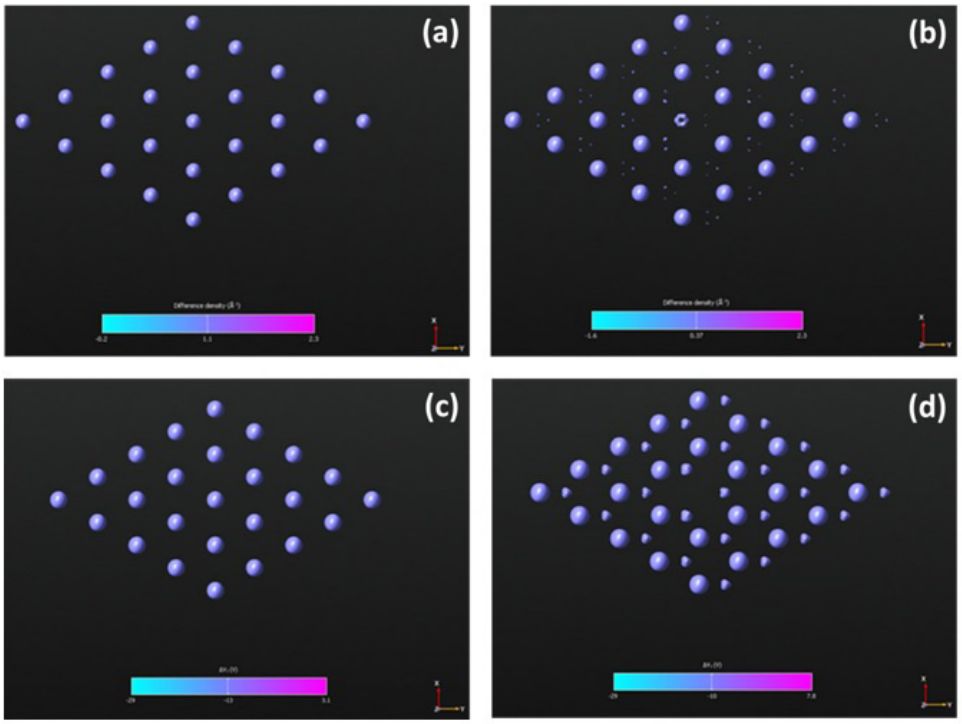

FIG. 2. Electron difference density diagrams of the (a) pristine and (b) Fe doped MoSeS; along with the electrostatic difference potential of the (c) pristine and (d) Fe doped structures

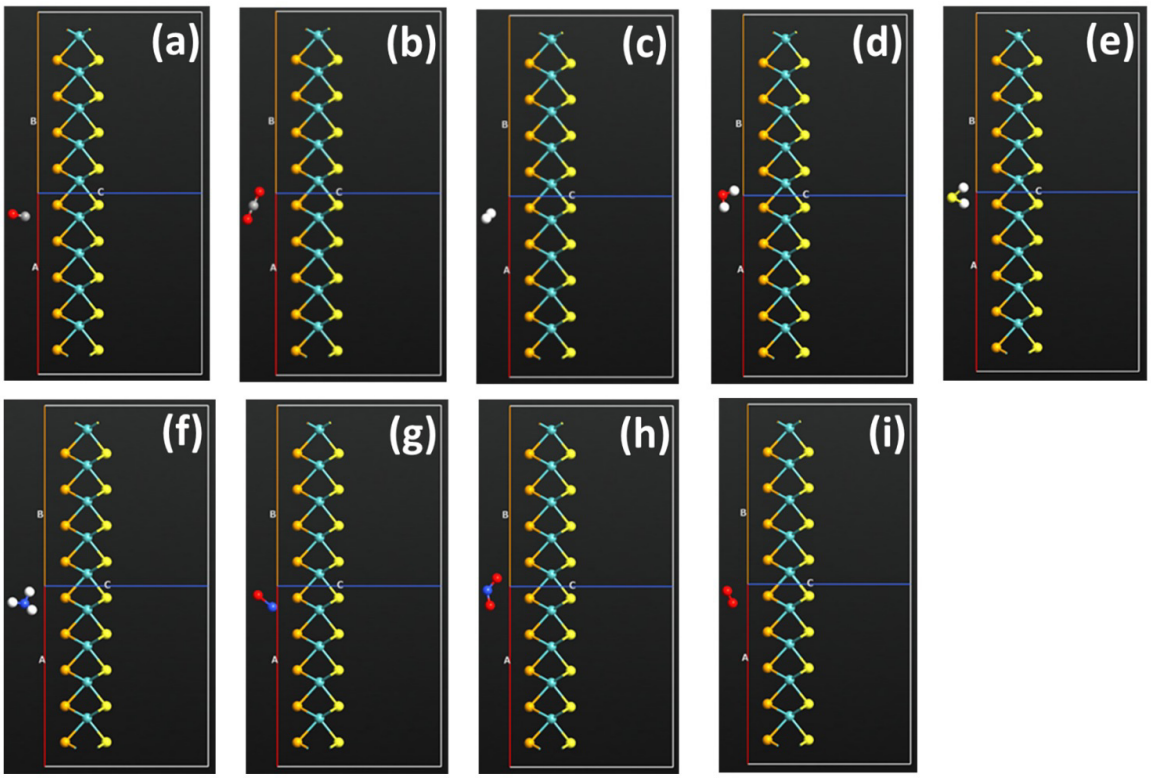

FIG. 3. Side view of the optimized pristine MoSeS structures after gas adsorption: a) CO, b) CO_2, c) H_2, d) H_2O, e) H_2S, f)NH_3, g) NO, h) NO_2 and i) O_2. The yellow-brown atoms are Se, yellow atoms are S, and the blue atoms are Mo

TABLE 1. Pristine MoSeS parameters before and after gas adsorption. E_g is the band gap energy, E_a and d are the adsorption energy and length, and Δq is the transferred charge

Structure	E_g (eV)	d (Å)	E_a (eV)	Δq (e)
MoSeS	1.375			
MoSeS–CO	1.368	2.98	−0.52	−0.03
MoSeS–CO_2	1.371	3.11	−0.30	0.022
MoSeS–H_2	1.369	3.11	−0.11	0.006
MoSeS–H_2O	1.368	2.69	−0.33	−0.009
MoSeS–H_2S	1.386	2.97	−0.41	−0.029
MoSeS–NH_3	1.370	2.90	−0.30	0.003
MoSeS–NO	0.275	2.67	−0.72	0.004
MoSeS–NO_2	0.614	3.06	−0.77	0.027
MoSeS–O_2	0.975	2.94	−1.36	−0.002

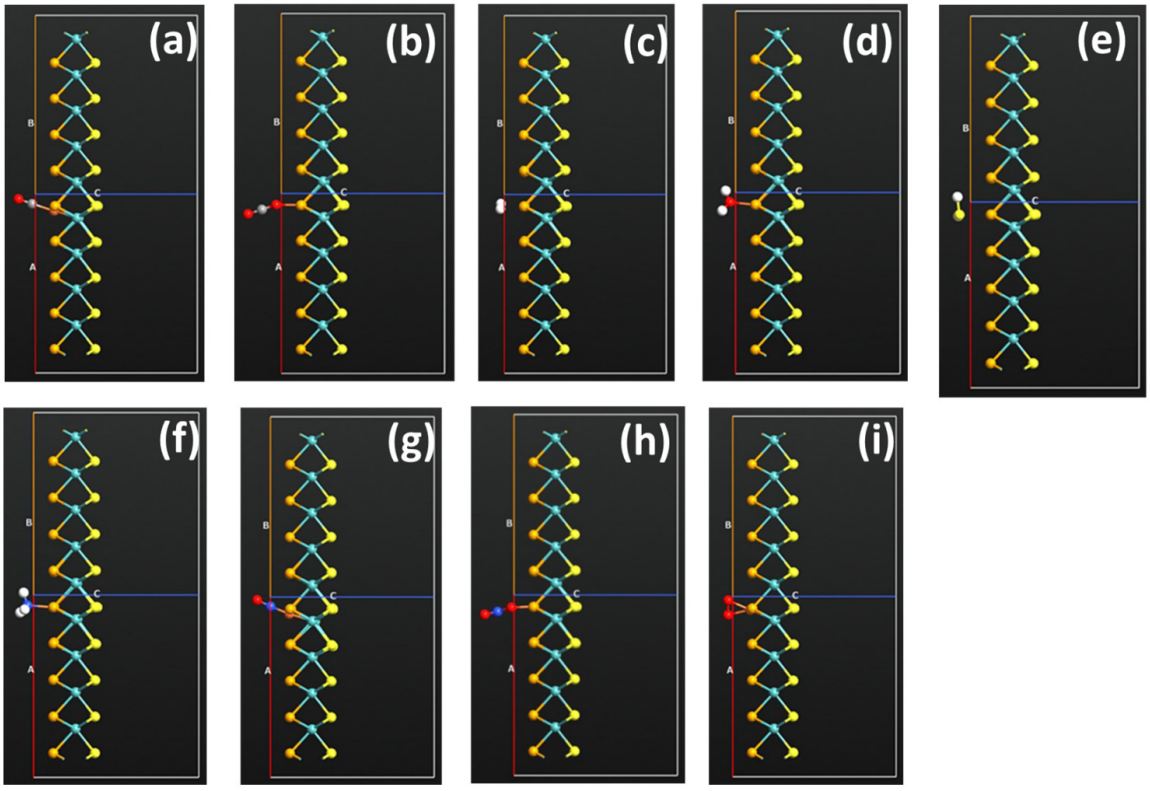

FIG. 4. Side view of the optimized Fe doped MoSeS structures after gas adsorption: a) CO, b) CO_2, c) H_2, d) H_2O, e) H_2S, f) NH_3, g) NO, h) NO_2, and i) O_2. The yellow-brown atoms are Se, yellow atoms are S, the blue atoms are Mo, and the brown atom is Fe (underneath Se)

Figures 5 and 6 present the band structures assigned to the optimized pristine and Fe doped MoSeS structures after gas adsorption. The figures reveal the introduction of new subbands between the valence and conduction bands due to gas adsorption as compared with the structures before gas adsorption (Fig. 1). Table 2 presents the band gap values of the Fe doped MoSeS structure before and after gas adsorption. The table illustrates a dramatic decrease in the band gap as compared with the pristine structure with a zero bandgap for the doped structure with H_2S gas adsorbed. Fe doped structures with CO_2, H_2, H_2O, H_2S, and NH_3 gases exhibit band gaps below 0.1 eV [39]. This switching between semiconducting to metallic or semimetallic characteristics is assigned to the newly introduced spin-polarized energy states. Figs. 5 and 6 present also the exchange splitting among spin-up and spin-down states near the Fermi level for the Fe dope MoSeS structure is indicating the spin-polarized density of states. The spin-polarized band gap energy of the Fe doped MoSeS structure before and after gas adsorption is presented in Table 2. The table reveals clear differences between the spin up and down states with a lower band gap for the spin down state. The spin down state exhibits semimetallic features mostly and mainly composed of mixing of the d_{xy}, d_{x2+y2}, and d_{z2} bands assigned to Mo atoms. The HOMO and LUMO corresponding to the spin up states consist of metallic d states along with mixed symmetry known for transition metal doping.

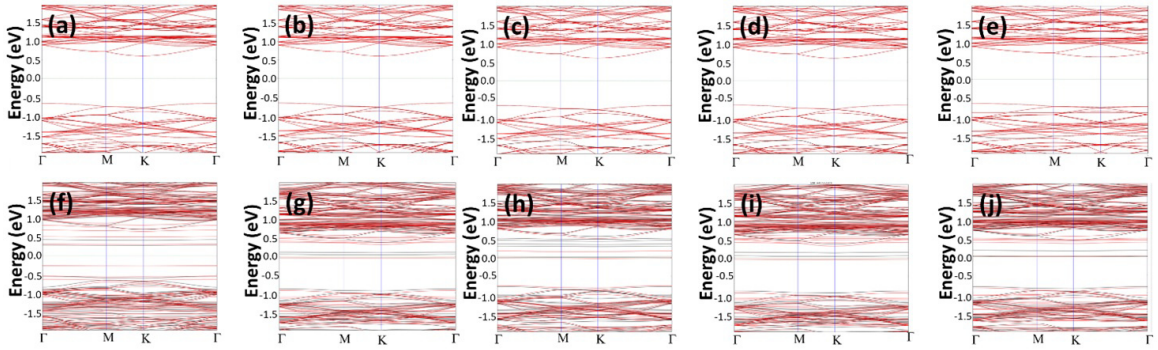

FIG. 5. The band structures for the optimized MoSeS structures: (a) – (e) pristine, and (f) – (j) Fe doped. (a) and (f) CO, (b) and (g) CO_2, (c) and (h) H_2, (d) and (i) H_2O, and (e) and (j) H_2S. The red lines are for spin up while the gray lines are for the spin down

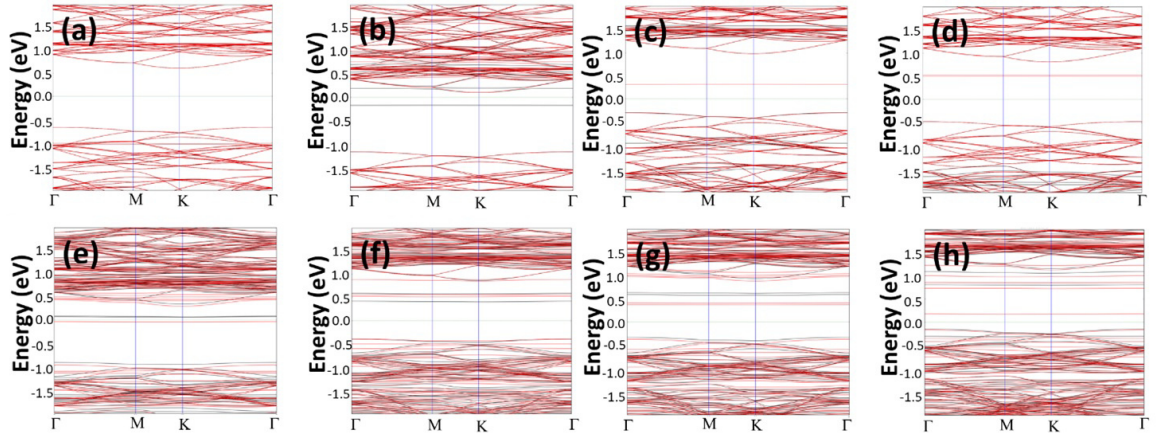

FIG. 6. The band structures for the optimized MoSeS structures: (a) – (d) pristine, and (e) – (h) Fe doped. (a) and (e) NH_3, (b) and (f) NO, (c) and (g) NO_2, and (d) and (h) O_2. The red lines are for spin up while the gray lines are for the spin down

The gas adsorption capacity of the MoSeS structures is revealed using the adsorption energy as presented in Tables 1 and 2. The tables indicate that the pristine structures exhibit a low magnitude of adsorption energy ($|E_a| \leq 1.36$ eV). The magnitude of adsorption energy of selected gases increases dramatically upon doping of MoSeS with Fe, with a maximum for NO. Herein, the adsorption energy of the structure for NO increases 4.9 times due to doping as compared with that of the pristine structure. For the doped structure, the minimum magnitude of adsorption energy is for H_2 and H_2S. The different adsorption energies for different gases on Fe doped structure illustrate its selective adsorption feature. Those results are in agreement with the observations of Figs. 3 and 4, where none of the gases is chemisorbed on the pristine structure. Additionally, for Fe doped structure, all of the gases are chemisorbed except H_2 and H_2S. It should be noted

TABLE 2. The parameters of Fe doped MoSeS before and after gas adsorption. E_g is the band gap energy, E_a and d are the adsorption energy and length, and Δq is the transferred charge. The table also shows the spin up and spin down band gaps (E_g^{up} and E_g^{down}, respectively) of the Fe doped MoSeS structure before and after gas adsorption

Structure	E_g (eV)	d (Å)	E_a (eV)	Δq (e)	E_g^{up} (eV)	E_g^{down} (eV)
MoSeS–Fe	0.114				0.87	0.21
MoSeS–Fe–CO	0.558	1.85	−2.33	0.069	0.84	0.60
MoSeS–Fe–CO_2	0.085	2.02	−1.00	−0.116	0.95	0.36
MoSeS–Fe–H_2	0.036	1.92	−0.45	−0.108	0.81	0.19
MoSeS–Fe–H_2O	0.082	2.07	−1.22	−0.109	1.10	0.36
MoSeS–Fe–H_2S	0.000	2.44	−1.40	−0.277	0.86	0.84
MoSeS–Fe–NH_3	0.099	2.10	−1.73	−0.242	1.00	0.94
MoSeS–Fe–NO	0.818	1.68	−3.51	0.08	0.82	0.93
MoSeS–Fe–NO_2	0.704	1.82	−2.86	0.401	0.92	0.75
MoSeS–Fe–O_2	0.330	1.90	−3.32	0.477	0.96	0.35

that the values of adsorption energy presented in the tables are negative, demonstrating the high adsorption capacity of MoSeS structures [24].

The charge transferred between a gas molecule and MoSeS structure is another indicator of its adsorption capacity. The charge transferred is presented in Tables 1 and 2 for both pristine and Fe doped MoSeS structures. Table 1 illustrates low charge transferred magnitudes for gases on pristine structure since none of them is chemisorbed. However, Table 2 reveals a clear increase in the magnitude of charge transferred for the Fe doped structure. CO, NO, NO_2, and O_2 gases exhibit positive values of charge transferred specifying that charge is transferred from the structure to the gas molecule. The combination of adsorption energy and length along with charge transferred reflects the increase of selective gas adsorption on the Fe doped MoSeS structure [40–42]. Accordingly, Fe doping of MoSeS structure is anticipated as an efficient approach for the production of selective gas sensors [43, 44]. Fe doping of MoSeS structure also modifies its energy levels and increases its interaction with the desirable gas molecules nearby the doping site [45].

The impact of Fe doping of MoSeS structure on the density of states is demonstrated in Fig. 7. The DOS of both spin states of pristine structure are identical. The figure shows direct modification of the energy states upon Fe doping. Different intensities of DOS for the two spin states appear for the doped structure. Specifically, the DOS increases for the Fe doped structure near the Fermi level at 0.07 eV with the introduction of new subbands and greater magnitude for the spin down state. At high and low energies (> 0.8 and < -0.8 eV), the DOS of Fe doped structure of up spin state exhibits lower intensity, in particular at 1.35, 3.2, −1.5, −2.3, −3.6, and −4.4. Generally, the band gap after gas adsorption of the doped structure is smaller than that of the pristine one. No major changes result in the band structure due to gas adsorption. Fig. 7h presents a clear modification of the band gap of the doped structure upon adsorption of NO, which has the highest adsorption energy. Herein, NO gas molecule exhibits one dangling bond with one unpaired electron of the N atom, while the NO_2 gas molecule exhibits one sigma and one half pi bonds for each pair of N–O bonds. Therefore, NO has more readiness to be adsorbed than NO_2. The modifications in the bandgap upon doping and gas adsorption presented in Table 2 are rationalized by the generation of new peaks in the DOS for the Fe doped MoSeS structure. Consequently, Fe doping of MoSeS and gas adsorption directly cause the observed DOS and band gap alterations.

The results in Figs. 5, 6, and 7 present the effect of gas adsorption on the spin resolved DOS for pristine and Fe doped MoSeS structures. The pristine structure has greater overall DOS near the Fermi level as compared with the Fe doped one. Most of the energy states in the conduction band near the Fermi level are assigned for spin up state. Fe doping of MoSeS structure engineers the band gap and transforms the structure from a semiconductor to a spin dependent metal or semimetal. Adsorption of gases generates new spin up/down states reference to the pristine structure. The DOS maximum intensity is mostly in the conduction band for the Fe doped MoSeS structure with exceptions based on the adsorbed gas type. The metallic and semimetallic states presented are assigned to the spin up state related to Fe dopant and Mo atoms adjacent to the doping site. The band gap near the Fermi level related to these atoms is assigned to the dispersive revealing of ferromagnetic coupling interactions triggered among the Fe dopant along with its mirror images.

Quantum confinement effect of charge carriers is reflected in their energy level hybridization (among s and d levels) for the structure atoms, molybdenum, selenium, and sulfur, thus, alterations in DOS are observed. Charge carriers are transferred between MoSeS structure and gas molecules that modify its DOS nearby the Fermi level, and transfer of

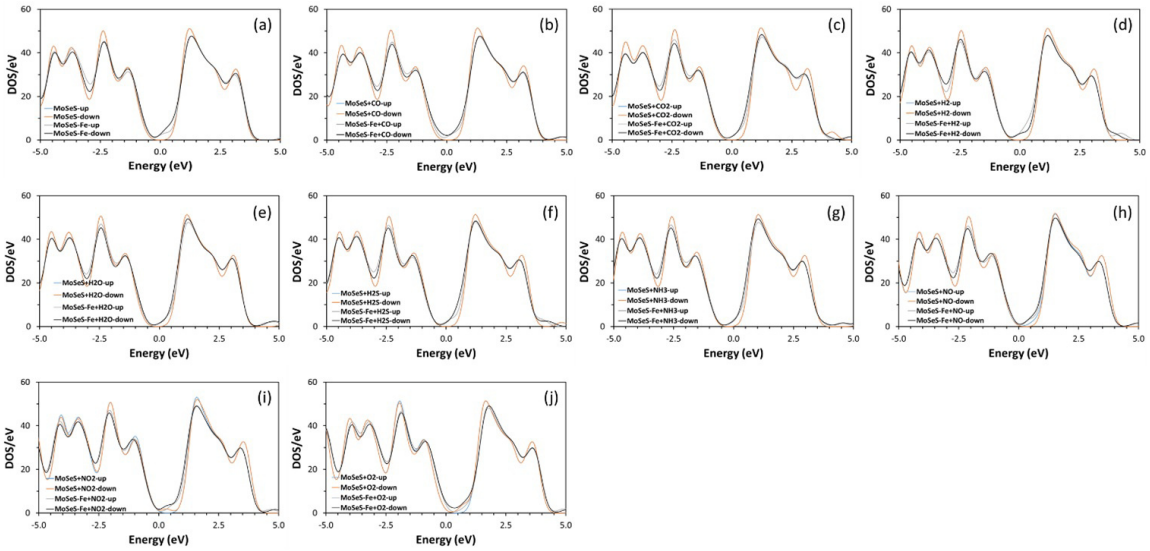

FIG. 7. Density of states for the optimized MoSeS structures (pristine and Fe doped): before gas adsorption a) and after adsorption of b) CO, c) CO_2, d) H_2, e) H_2O, f) H_2S, g) NH_3, h) NO, i) NO_2, and j) O_2

charge occurs to the p energy levels of both selenium and sulfur. The shift in Fermi level and orbital hybridization (Figs. 5, 6, and 7) reflect Fe doping effect of the MoSeS structure, and it is altered due to gas adsorption. Fe doped MoSeS structure reveals flat bands approximately near the Fermi level signifying its robust gas adsorption feature. The primary source of alteration of energy states for MoSeS structure is the occupied DOS subsequent to gas adsorption [46]. Therefore, the presented results illustrate that Fe doping of MoSeS structure is an efficient approach for switching between the metallic/semimetallic and semiconducting behavior based on changing the spin orientation, and promoting its gas adsorption efficiency.

The decrease in band gap energy upon doping and gas adsorption is assigned to the orbitals' hybridization near the bottom and top of the conduction and valence bands, respectively, with the d orbitals of the Fe atom [47]. The improvement in gas adsorption is attributed to charge transfer amongst the gas molecules and Fe doped MoSeS which results from modifying charge concentration decreasing the resistance as demonstrated by the decrease in the band gap. The enhanced sensor response of the doped structure is allocated to its exceptional reactivity and affinity towards gas molecules [48].

The improvement of the selective gas adsorption upon Fe doping of MoSeS structure can be invested for gas sensing applications. Herein, a sensor response (S) is evaluated using [49]:

$$S = \left| \frac{\sigma_i - \sigma_f}{\sigma_f} \right|, \tag{3}$$

where σ_i and σ_f represent the structure conductivities before and after gas adsorption, respectively. The conductivity can be determined using [43]:

$$\sigma_{i,f} = \sigma_0 e^{-\frac{E_g}{2k_B T}}, \tag{4}$$

where σ_0 is a constant that is independent of temperature, $k_B = 8.62 \times 10^{-5}$ eV.K$^(-1)$ which is known as Boltzmann constant, and T is the MoSeS temperature (set to 300 K). The equations could be used to provide a qualitative indication regarding the sensor response (since the evaluated conductivity is a theoretical estimate value). The results indicate that the sensor response of Fe doped MoSeS structure increases by a factor between 1.8 – 20.4 times for the gases compared with the corresponding pristine structure (with the exception for NO, NO_2, and O_2 where the model did not produce rational results due to the relatively large band gap). This brilliant sensor response validates the outstanding improvement of selective gas adsorption as a result of doping which supports the computational results. Therefore, Fe doping of MoSeS dichalcogenide is a potential approach for the fabrication of half metallic structures that are sensitive and selective and can be utilized for the production of gas detectors.

4. Conclusion

The effect of Fe doping of MoSeS dichalcogenide structure on its half metallic transformation and adsorption of multiple gases have been investigated using first principles computations and density functional theory (DFT). The band gap variation of the spin-polarized density of states has been explored through density of states (DOS), and band structure. The capacity of gas adsorption has been evaluated by examining the gas adsorption energy and length along with the charge

relocated between gas molecules and the structure. Fe doping of MoSeS dichalcogenide generated significant adjustments of the band gap so that the structure could be transformed from semiconductor into metallic or semimetallic. The spin down state exhibited semimetallic features mostly. The HOMO and LUMO corresponding to the spin up states consisted of metallic d states along with mixed symmetry known for transition metal doping. Doping of MoSeS dichalcogenide improved its selective gas adsorption with a maximum magnitude of adsorption energy and reduced adsorption length for NO that caused its chemisorption. The magnitude of the adsorption energy of the structure for NO increased 4.9 times due to doping, while the doped structure had the lowest adsorption energies for H_2 and H_2S. Therefore, Fe doping of MoSeS dichalcogenide is a promising approach for its band gap engineering and control of its selective gas adsorption.

References

[1] Novoselov K.S., et al. Electric field effect in atomically thin carbon films. *Science*, 2004, **306**(5696), P. 666–669.

[2] Zheng N., Bu X., and Feng P. Synthetic design of crystalline inorganic chalcogenides exhibiting fast-ion conductivity. *Nature*, 2003, **426**(6965), P. 428–432.

[3] Ayesh A.I. Investigation of BN modified graphene nanoribbon for gas adsorption applications: DFT study. *Chinese Journal of Physics*, 2023, **85**, P. 649–659.

[4] Amiri V., et al. Nanostructured metal oxide-based acetone gas sensors: A review. *Sensors*, 2020, **20**(11), P. 3096.

[5] Salih E. and Ayesh A.I. First principle study of transition metals codoped MoS_2 as a gas sensor for the detection of NO and NO_2 gases. *Physica E: Low-dimensional Systems and Nanostructures*, 2021, **131**, P. 114736.

[6] Zhou J., et al. A library of atomically thin metal chalcogenides. *Nature*, 2018, **556**(7701), P. 355–359.

[7] Mouw C.B., et al. Aquatic color radiometry remote sensing of coastal and inland waters: Challenges and recommendations for future satellite missions. *Remote sensing of environment*, 2015, **160**, P. 15–30.

[8] Ayesh A.I. Investigation of NH3 adsorption on noble metal modified $MoSe_2$. *Physica E: Low-dimensional Systems and Nanostructures*, 2022, **139**, P. 115188.

[9] Abu-Hani A.F., et al. Low-temperature and fast response H2S gas sensor using semiconducting chitosan film. *Sensors and Actuators B: Chemical*, 2017, **253**, P. 677–684.

[10] Niu F., et al. Si-doped graphene nanosheets for NOx gas sensing. *Sensors and Actuators B: Chemical*, 2021. **328**, P. 129005.

[11] Felegari Z., Hamedani S. Adsorption properties of the phosgene molecule on pristine graphyne, BN-and Si-doped graphynes: DFT study. *Results in Physics*, 2017, **7**, P. 2626–2631.

[12] Son Y.-W., Cohen M.L., Louie S.G. Half-metallic graphene nanoribbons. *Nature*, 2006, **444**(7117), P. 347–349.

[13] Bergman G. Influence of spin-orbit coupling on weak localization. *Physical Review Letters*, 1982, **48**(15), P. 1046.

[14] Picozzi S., Freeman A.J. Polarization reduction in half-metallic Heusler alloys: the effect of point defects and interfaces with semiconductors. *Journal of Physics: Condensed Matter*, 2007, **19**(31), P. 315215.

[15] Miura Y., Nagao K., Shirai M. Atomic disorder effects on half-metallicity of the full-Heusler alloys Co_2 $(Cr_{1-x}Fe_x)$ Al: A first-principles study. *Physical Review B*, 2004, **69**(14), P. 144413.

[16] Liu Z., et al. Atomically Substitutional Engineering of Transition Metal Dichalcogenide Layers for Enhancing Tailored Properties and Superior Applications. *Nano-Micro Letters*, 2024, **16**(1), P. 1–37.

[17] Khan S., Feng Y.-P., Tit N. Synergetic effects of combining TM single-and double-atom catalysts embedded in C_2N on inducing half-metallicity: DFT study. *2D Materials*, 2022, **10**(1), P. 015016.

[18] Elphick K., et al. Heusler alloys for spintronic devices: review on recent development and future perspectives. *Science and Technology of Advanced Materials*, 2021, **22**(1), P. 235–271.

[19] Sriram K., et al. Structural Phase Engineering of $(\alpha + \beta)$-W for a Large Spin Hall Angle and Spin Diffusion Length. *The Journal of Physical Chemistry C*, 2023, **127**(46), P. 22704–22712.

[20] Ahn Y. Progress and prospects in two-dimensional magnetism of van der Waals materials. *Progress in Quantum Electronics*, 2024, P. 100498.

[21] Ma J., et al. Enhancing photocatalytic overall water-splitting performance on dual-active-sites of the Co–P@ MoS 2 catalysts: a DFT study. *Physical Chemistry Chemical Physics*, 2023, **25**(32), P. 21554–21561.

[22] Liu Q., Zhao X., Chen X. Single transition metal-decorated C4N/MoS2 heterostructure for boosting oxygen reduction, oxygen evolution, and hydrogen evolution. *Journal of Colloid and Interface Science*, 2023, **648**, P. 787–797.

[23] Alfalasi W., Feng Y.P., Tit N. Designing a functionalized 2D-TMD (MoX_2, X= S, Se) hosting half-metallicity for selective gas-sensing applications: Atomic-scale study. *Acta Materialia*, 2023, **246**, P. 118655.

[24] Salih E., Ayesh A.I. Enhancing the Sensing Performance of Zigzag Graphene Nanoribbon to Detect NO, NO_2, and NH_3 Gases. *Sensors*, 2020, **20**(14), P. 3932.

[25] Salih E., Ayesh A.I. Computational study of metal doped graphene nanoribbon as a potential platform for detection of H_2S. Materials Today Communications, 2021, **26**, P. 101823.

[26] Salah B., Ayesh A.I. Fabrication of H_2S sensitive gas sensors formed of SnO_2-Fe_2O_3 composite nanoparticles. *Materials Chemistry and Physics*, 2021, P. 124597.

[27] Salih E., Ayesh A.I. Sensitive SO_2 gas sensor utilizing Pt-doped graphene nanoribbon: First principles investigation. *Materials Chemistry and Physics*, 2021, **267**, P. 124695.

[28] Salih E., Ayesh A.I. DFT investigation of H_2S adsorption on graphenenanosheets and nanoribbons: Comparative study. *Superlattices and Microstructures*, 2020, **146**, P. 106650.

[29] Ayesh A.I. Effect of CuOx additive site to graphene nanoribbon on its adsorption for hydrogen sulfide. *Results in Physics*, 2021, **24**, P. 104199.

[30] Perdew J.P., Burke K., Ernzerhof M. Generalized gradient approximation made simple. *Physical Review Letters*, 1996, **77**(18), P. 3865.

[31] Grimme S. Semiempirical GGA-type density functional constructed with a long-range dispersion correction. *Journal of computational chemistry*, 2006, **27**(15), P. 1787–1799.

[32] Salih E., Ayesh A.I. Pt-doped armchair graphene nanoribbon as a promising gas sensor for CO and CO_2: DFT study. *Physica E: Low-dimensional Systems and Nanostructures*, 2021, **125**, P. 114418.

[33] Liu D., et al. Adsorption of SF_6 decomposition components over Pd (1 1 1): A density functional theory study. *Applied Surface Science*, 2019. **465**, P. 172–179.

[34] Salih E., Ayesh A.I. CO, CO_2, and SO_2 detection based on functionalized graphene nanoribbons: First principles study. *Physica E: Low-dimensional Systems and Nanostructures*, 2020, P. 114220.

[35] Salih E., Ayesh A.I. First principle investigation of H_2Se, H_2Te and PH_3 sensing based on graphene oxide. *Physics Letters A*, 2020, **384**(29), P. 126775.
[36] Mulliken R.S. Electronic population analysis on LCAO–MO molecular wave functions. I. *The Journal of Chemical Physics*, 1955, **23**(10), P. 1833–1840.
[37] Ribeiro-Soares J., et al. Group theory analysis of phonons in two-dimensional transition metal dichalcogenides. *Physical Review B*, 2014, **90**(11), P. 115438.
[38] Lin Z., Ye J., An Y. Tunable electronic structures, half-metallicity and optical properties in Fe-NM (NM=B, C, N) co-doped monolayer 2H–$MoSe_2$. *Journal of Alloys and Compounds*, 2019, **805**, P. 578–584.
[39] Padilla V.E.C., et al. Studies of hydrogen sulfide and ammonia adsorption on P-and Si-doped graphene: density functional theory calculations. *Journal of Molecular Modeling*, 2019, **25**(4), P. 94.
[40] Pakornchote T., et al. Phase stabilities and vibrational analysis of hydrogenated diamondized bilayer graphenes: A first principles investigation. *Carbon*, 2019, **146**, P. 468–475.
[41] Ahangari M.G., et al. Effect of various defects on mechanical and electronic properties of zinc-oxide graphene-like structure: A DFT study. *Vacuum*, 2019. **165**, P. 26–34.
[42] Gao X., et al. Adsorption of SO_2 molecule on Ni-doped and Pd-doped graphene based on first-principle study. *Applied Surface Science*, 2020, P. 146180.
[43] Liu, T., et al. Al-Doped $MoSe_2$ Monolayer as a Promising Biosensor for Exhaled Breath Analysis: A DFT Study. *ACS Omega*, 2020, **6**(1), P. 988–995.
[44] Zhang D., et al. Fabrication of Pd-Decorated $MoSe_2$ Nanoflowers and Density Functional Theory Simulation Toward Ammonia Sensing. *IEEE Electron Device Letters*, 2019, **40**(4), P. 616–619.
[45] Ma S., et al. A first-principles insight into Pd-doped $MoSe_2$ monolayer: A toxic gas scavenger. *Physics Letters A*, 2019, **383**(30), P. 125868.
[46] Walia G.K., Randhawa D.K.K. First-principles investigation on defect-induced silicene nanoribbons—A superior media for sensing NH_3, NO_2 and NO gas molecules. *Surface Science*, 2018, **670**, P. 33–43.
[47] Chen H., et al. Adsorption of NO and NO_2 on MoSeS/GaN heterojunction: a first-principles study. *Physica Scripta*, 2024, **99**(2), P. 025981.
[48] Hui W., Chang G., Gao W. Exploring the electronic and magnetic properties of noble metal (Pd, Pt, Au) adsorbed $MoSe_2$ monolayers and their performance towards sensing gas molecules. *Physica E: Low-dimensional Systems and Nanostructures*, 2020, **122**, P. 114167.
[49] Ayesh A.I., et al. Production of sensitive gas sensors using CuO/SnO_2 nanoparticles. *Applied Physics A*, 2019. **125**(8), P. 1–8.

Submitted 21 June 2025; revised 26 June 2025; accepted 7 July 2025

Information about the authors:

Ahmad I. Ayesh – Department of Physics and Materials Sciences, College of Arts and Sciences, Qatar University, P. O. Box 2713, Doha, Qatar; ORCID 0000-0002-0442-5941; ayesh@qu.edu.qa

Conflict of interest: the authors declare no conflict of interest.